

3D SA-UNET: 3D SPATIAL ATTENTION UNET WITH 3D ATROUS SPATIAL PYRAMID POOLING FOR WHITE MATTER HYPERINTENSITIES SEGMENTATION

Changlu Guo, Haoyu Chen, Yugen Yi

<https://github.com/clguo/3DSAUNet>

ABSTRACT

White Matter Hyperintensity (WMH) is an imaging feature related to various diseases such as dementia and stroke. Accurately segmenting WMH using computer technology is crucial for early disease diagnosis. However, this task remains challenging due to the small lesions with low contrast and high discontinuity in the images, which contain limited contextual and spatial information. To address this challenge, we propose a deep learning model called 3D Spatial Attention U-Net (3D SA-UNet) for automatic WMH segmentation using only Fluid Attenuation Inversion Recovery (FLAIR) scans. The 3D SA-UNet introduces a 3D Spatial Attention Module that highlights important lesion features, such as WMH, while suppressing unimportant regions. Additionally, to capture features at different scales, we extend the Atrous Spatial Pyramid Pooling (ASPP) module to a 3D version, enhancing the segmentation performance of the network. We evaluate our method on publicly available dataset and demonstrate the effectiveness of 3D spatial attention module and 3D ASPP in WMH segmentation. Through experimental results, it has been demonstrated that our proposed 3D SA-UNet model achieves higher accuracy compared to other state-of-the-art 3D convolutional neural networks.

Index Terms— White Matter Hyperintensity, Deep Learning, Spatial Attention, 3D SA-UNet, ASPP

1. INTRODUCTION

Patients who exhibit symptoms such as aging, stroke, and dementia often suffer from small-vessel disease, and white matter hyperintensity (WMH) is one of the features of small-vessel disease that is clearly visible on MRI images. In recent years, the quantification of the location, shape and volume of high white matter hyperintensity has been conducive to the diagnosis, prognosis and treatment monitoring of neurodegenerative diseases such as stroke and dementia [1]. Although visual grading by trained experts remains the most widely used method of studying WMH, it has limitations such as time-consuming and subjective, so automated and accurate segmentation of WMH is particularly important.

With the widespread application of deep learning in medical image processing, the automatic segmentation of WMH has also benefited, with popular models like U-Net [5] being employed for this task. Guerreroa et al.[2] proposed a network called uResNet, which combines the strengths of ResNet[6] and U-Net for segmenting hyperintensities using 2D image patches. Li et al.[4] proposed an ensemble method that combines multiple U-Nets and achieved first place in the WMH Segmentation Challenge at MICCAI 2017[3]. Vaanathi et al. [7] devised an ensemble triplanar network that integrated the predictions from three distinct planes of MRI images to achieve a precise segmentation of white matter hyperintensities (WMH). However, it is easy to find that few 3D convolutional neural networks have been applied to this work, mainly due to the low contrast and high discontinuity of small lesion areas in WMH images, containing poor spatial and contextual information, as well as the poor imaging resolution and large spatial resolution variation of these images along the z -direction, which limit the use of 3D deep learning models[4]. To tackle the aforementioned challenges, we employ a bold design strategy by using a $3 \times 3 \times 1$ convolution kernel instead of the traditional $3 \times 3 \times 3$ convolution kernel in both the 3D encoder and decoder, allowing the network to focus on image information in the x and y directions. Furthermore, in the bottleneck block between the encoder and decoder, we retain the design of 3D convolution to preserve the network’s ability to capture essential 3D features. To further enhance the network’s capability to capture multi-scale information, we introduce an extended version of 3D ASPP within the bottleneck block. This extension enables the network to learn and integrate multi-scale information more effectively. Finally, unlike the skip connections in U-Net, which simply concatenate low-level and high-level features without fully utilizing spatial relationships, we have incorporated a 3D Spatial Attention Module within the skip connections. This addition enhances the network’s ability to focus on crucial spatial relationships in the images, allowing it to effectively capture relevant context and spatial dependencies between features. Through conducting ablation experiments and comparing with state-of-the-art methods, we validate the effectiveness of our design and the superiority of the 3D SA-UNet.

¹<https://github.com/hjkuijf/wmhchallenge/blob/master/evaluation.py>

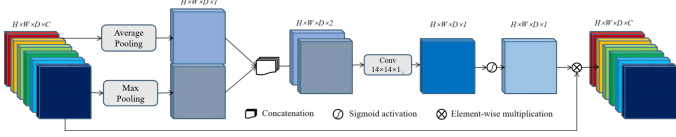


Fig. 1. Diagram of the 3D Spatial Attention Module.

2. METHODS

2.1. 3D Spatial Attention Module

Spatial Attention mechanisms enable the network to amplify significant features and dampen or diminish insignificant ones. Spatial Attention Module is proposed as part of convolutional block attention module (CBAM)[8], and SA-UNet [9] applies spatial attention to retinal vessel segmentation in 2D fundus image, making the segmentation performance reached state-of-the-art. Inspired by the above work, we introduce a 3D Spatial Attention Module (3D SAM) to improve the WMH segmentation performance of 3D MRI images. In order to obtain the spatial attention map, 3D SAM utilizes both max-pooling and average-pooling operations along the channel axis. These operations are then concatenated to generate an optimized feature descriptor, as depicted in Figure 1. Mathematically, the input feature map $F \in R^{H \times W \times D \times C}$ undergoes channel-wise average-pooling and max-pooling operations, resulting in the generation of outputs $F_{ap} \in R^{H \times W \times D \times 1}$ and $F_{mp} \in R^{H \times W \times D \times 1}$, respectively. Afterwards, a convolutional layer is applied to the concatenated feature descriptor, and the output is then passed through the Sigmoid activation function to generate a 3D spatial attention map $M^{sa} \in R^{H \times W \times D \times 1}$. In short, the output feature map $F^{sa} \in R^{H \times W \times D \times C}$ of 3D SAM can be calculated as:

$$\begin{aligned}
 F^{sa} &= F \times M^{sa} \\
 &= F \times \sigma(f^{14 \times 14 \times 1}([F_{ap}; F_{mp}])) \\
 &= F \times \sigma(f^{14 \times 14 \times 1}([Avg(F); Max(F)]))
 \end{aligned} \quad (1)$$

where $f^{14 \times 14 \times 1}(\bullet)$ refers to a 3D convolutional layer, and $\sigma(\bullet)$ means Sigmoid function.

2.2. 3D Atrous Spatial Pyramid Pooling

Atrous Spatial Pyramid Pooling (ASPP) is a widely used module in deep learning models, originally introduced in DeepLab[10] for 2D image semantic segmentation. ASPP operates on the output feature maps of a convolutional neural network (CNN), aiming to aggregate information from multiple receptive fields with different dilation rates. This enables the model to capture information at various scales, enhancing its ability to accurately segment objects or regions in images. Therefore, in this task, we enhance the ASPP module by expanding it to 3D, replacing Batch Normalization (BN) with

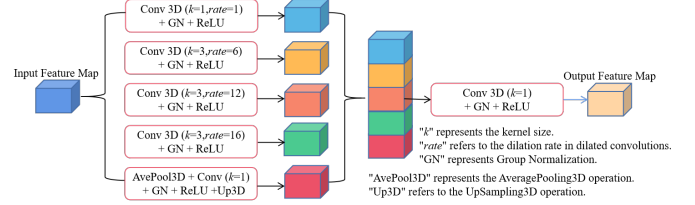


Fig. 2. Diagram of the 3D Atrous Spatial Pyramid Pooling (3D ASPP).

Group Normalization (GN)[11], and referring to it as “3D ASPP”. 3D ASPP consists of parallel convolution operations, with each branch utilizing a different dilation rate, as depicted in Figure 2. By leveraging the multi-scale contextual information, we argue that the 3D ASPP can improve the model’s understanding of the spatial context, leading to more precise segmentation results.

2.3. 3D SA-UNet

As with the 3D U-Net architecture, our model also adopts the classic encoder-decoder structure, as illustrated in Figure 3. To efficiently handle a minibatch size of 4 for this task, we incorporate Group Normalization (GN) between the convolutional layer and the ReLU layer, as GN has shown to exhibit smaller errors with this minibatch size. Considering the poor imaging resolution along the z -axis and the large spatial resolution variations in WMH images, the convolution layers in both the encoder and decoder parts of the model use a kernel size of $3 \times 3 \times 1$. However, the bottleneck block between the encoder and decoder retains the use of a $3 \times 3 \times 3$ convolution kernel to preserve the network’s ability to capture essential 3D features. Similarly, both the encoder’s down-sampling layer and the decoder’s up-sampling layer are implemented using a kernel size of $2 \times 2 \times 1$. Additionally, we introduce a 3D ASPP between the encoder and decoder, which enables the network to learn and integrate multi-scale information more effectively. Moreover, we extend the utilization of 3D SAM to the skip connections, aiming to enhance the network’s ability to focus on crucial spatial relationships in the images. This allows the model to effectively capture relevant context and spatial dependencies between features.

3. EXPERIMENTS AND RESULTS

3.1. Experiments

To evaluate the performance of our proposed 3D SA-UNet, we conduct experiments on the MICCAI 2017 WMH Segmentation Challenge Dataset, specifically for the task of White Matter Hyperintensities (WMH) Segmentation. We utilized the FLAIR data from this dataset, which comprises 60 training images acquired using three distinct scanners.

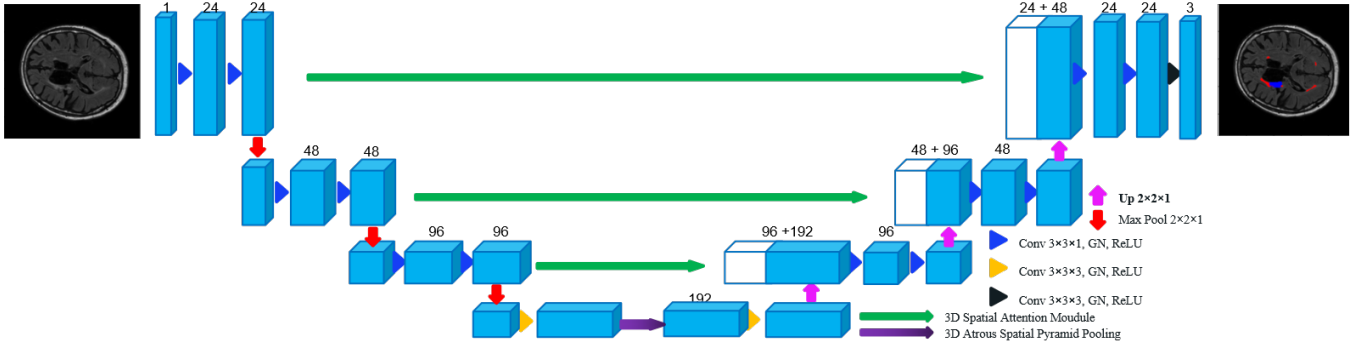


Fig. 3. Diagram of the 3D SA-UNet.

Additionally, the dataset includes 110 test images acquired using five different scanners. Among the test scanners, three of them correspond to the same scanners utilized during training, while the remaining two scanners were not employed in the training phase. Each image is accompanied by manually annotated ground truth, with labels divided into 0 for background, 1 for WMH (White Matter Hyperintensities), and 2 for other pathologies, for further details about the dataset, please refer to MICCAI 2017 WMH Segmentation Challenge[3]. To enhance the robustness of the network, we employ multiple augmentation techniques, including rotation, random flipping, and random transposition, as well as channel shift, bias field correction, elastic deformations, and motion ghosting. All models in this paper were trained from scratch using a combined loss function (cross-entropy and Dice loss) and optimized with the Adam method, initialized with a learning rate of 0.001. We quantitatively evaluate the performance using several metrics and the *code*¹ provided by the challenge’s official evaluation, including Dice Similarity Coefficient (DICE), Average Volume Difference (AVD), and F1-score (F1).

3.2. Ablation Studies

To verify the significance of each component in the 3D SA-UNet for this task, we employ the traditional U-shaped network with Batch Normalization and the initial convolutional layer consisting of 24 channels as our Backbone. Firstly, we compare the “Backbone with (3,3,3) & (2,2,2)” and the “Backbone with (3,3,1) & (2,2,1)”. The main difference between them lies in the convolutional kernel size of the encoder and the decoder. The former uses a kernel size of (3,3,3), while the latter uses (3,3,1). Additionally, there is a difference in the size of the down-sampling layers and the up-sampling layers. The former has a size of (2,2,2), whereas the latter has a size of (2,2,1). As we observe from the results in the first two rows of table 1, “Backbone with (3,3,1) & (2,2,1)” compared to “Backbone with (3,3,3) & (2,2,2)” was significantly improved in all metrics, especially F1, which

improved by more than 20%, and these findings substantiate that the adjustments align with the characteristics of the input data. Secondly, we compare the “Backbone with (3,3,1) & (2,2,1)” and the “Backbone* with GN” to validate the effectiveness of Group Normalization (GN). Here, “Backbone* with GN” represents the basic architectural design that is identical to “Backbone with (3,3,1) & (2,2,1)” but with the replacement of BN by GN. From the results, it can be observed that “Backbone* with GN” achieves better performance in all metrics compared to “Backbone with (3,3,1) & (2,2,1)”, indicating that Group Normalization (GN) is beneficial for this task. Third, we separately add 3D SAM and 3D ASPP to “Backbone* with GN”, and from the results, it can be concluded that both 3D ASPP and 3D SAM can improve segmentation performance. Finally, through the combination of 3D SAM and 3D ASPP, our 3D SA-Net is finally built, which achieves the highest DICE of 0.79 and F1 of 0.76, although AVD is not the lowest, it is also comparable. These results demonstrate the effectiveness of the 3D SA-UNet design for this task. We believe that the above is enough to demonstrate that the design of 3D SA-UNet is effective in this work.

Table 1. Ablation Experiments on MICCAI Challenge.

Models	DICE	AVD ↓	F1
Backbone with (3,3,3) & (2,2,2)	0.66	0.356	0.46
Backbone with (3,3,1) & (2,2,1)	0.75	0.225	0.68
Backbone* with GN	0.78	0.172	0.71
Backbone* with GN+3D ASPP	0.77	0.170	0.71
Backbone* with GN+3D SAM	0.78	0.182	0.75
3D SA-UNet	0.79	0.174	0.76

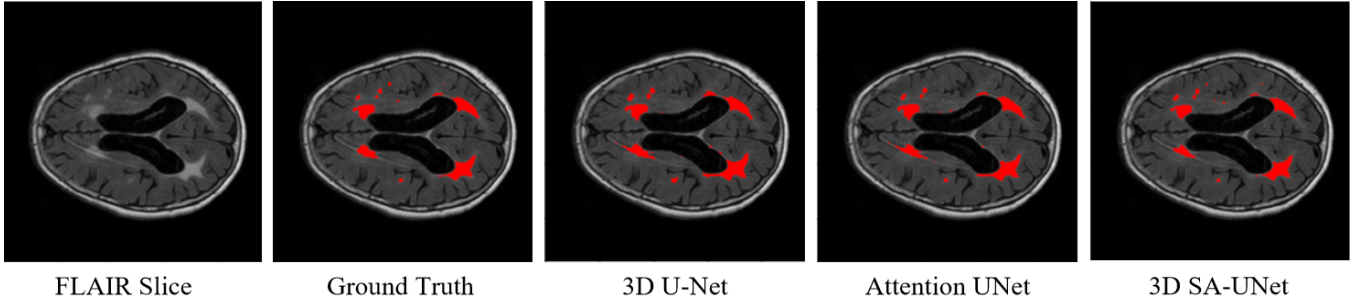


Fig. 4. Visual comparison of segmentation results for one sample from the testset.

3.3. Comparison with other state-of-the-art models

It is well known that since the release of U-Net, many neural networks for medical image segmentation have been variants of U-Net. This trend extends to 3D images as well, where a range of 3D models based on U-Net have been proposed, including 3D-UNet[12], Attention UNet[13] and so on. Additionally, We compare our results with the Challenge Winner[4], which uses an ensemble of 2D U-Nets with both T1 and FLAIR imaging modalities and achieved the best performance in the WMH Segmentation Challenge. Quantitatively, as shown in Table 2, our proposed method achieves state-of-the-art performance. Compared to 3D U-UNet and Attention UNet, 3D SA-UNet outperforms in all metrics. When compared to the Challenge Winner, 3D SA-UNet achieves the smallest AVD of 0.174, a decrease of nearly 4.5%, the same F1 of 0.76, and comparable Dice of 0.79. Visually, as depicted in Fig. 4, 3D U-Net and Attention UNet struggle to identify small-volume WMH areas and exhibit missegmentation. In contrast, 3D SA-UNet accurately identifies more small-volume WMH regions and exhibits fewer missegmentations.

In addition, we present the results of 3D SA-UNet on images from five different scanners in the testset, as shown in Table 3. The results demonstrate that the model remains effective even on images from scanners that were not included in the training data, showcasing the robustness of 3D SA-UNet.

Table 2. Comparison with Other State-of-the-art Models.

Models	DICE	AVD ↓	F1
3D U-Net	0.71	0.289	0.53
Attention UNet	0.74	0.206	0.57
MICCAI Challenge Winner	0.80	0.219	0.76
3D SA-UNet	0.79	0.174	0.76

Table 3. Segmentation Performance of 3D SA-UNet on Different Scanners.

Scanners	DICE ↓	AVD ↓	F1
Utrecht (n = 30)	0.79	0.151	0.71
Singapore (n = 30)	0.82	0.156	0.78
Amsterdam Philips (n=10)	0.72	0.167	0.73
Amsterdam GE3T 01 (n=30)	0.79	0.201	0.79
Amsterdam GE1.5T (n=10)	0.77	0.225	0.80
Average	0.79	0.174	0.76

4. CONCLUSION

In this paper, we present a novel automated 3D convolutional neural network, referred to as 3D SA-UNet, specifically crafted for White Matter Hyperintensity (WMH) segmentation using only FLAIR scans. We assess the impact of each architectural component through ablation experiments, aiming to gauge the effectiveness of each element within the 3D SA-UNet design. To illustrate the superiority of 3D SA-UNet, we carry out comparative experiments with 3D U-Net and Attention UNet. Additionally, we compare our results to the best-performing method in the WMH Segmentation Challenge. Our key findings can be summarized as follows: (1) FLAIR imaging alone proves to be sufficient for accurate WMH segmentation; (2) Properly adapting convolutional kernel sizes based on the input image features is effective, particularly when dealing with the substantial spatial resolution variation along the z-axis in 3D medical images; (3) Focusing on spatial correlations and incorporating multi-scale information contributes significantly to enhancing model performance; (4) 3D SA-UNet exhibits robust performance across diverse scanners and imaging protocols; (5) Comparing our results with the state-of-the-art 2D methods, we demonstrate that our proposed 3D approach is equally effective for WMH segmentation.

5. REFERENCES

- [1] Wardlaw, J.M., Valdés Hernández, M.C. and Muñoz-Maniega, S., 2015. What are white matter hyperintensities made of? Relevance to vascular cognitive impairment. *Journal of the American Heart Association*, 4(6), p.e001140.
- [2] Guerrero, R., Qin, C., Oktay, O., Bowles, C., Chen, L., Joules, R., Wolz, R., Valdés-Hernández, M.D.C., Dickie, D.A., Wardlaw, J. and Rueckert, D., 2018. White matter hyperintensity and stroke lesion segmentation and differentiation using convolutional neural networks. *NeuroImage: Clinical*, 17, pp.918-934.
- [3] Kuijff, H.J., Biesbroek, J.M., De Bresser, J., Heinen, R., Andermatt, S., Bento, M., Berseth, M., Belyaev, M., Cardoso, M.J., Casamitjana, A. and Collins, D.L., 2019. Standardized assessment of automatic segmentation of white matter hyperintensities and results of the WMH segmentation challenge. *IEEE transactions on medical imaging*, 38(11), pp.2556-2568.
- [4] Li, H., Jiang, G., Zhang, J., Wang, R., Wang, Z., Zheng, W.S. and Menze, B., 2018. Fully convolutional network ensembles for white matter hyperintensities segmentation in MR images. *NeuroImage*, 183, pp.650-665.
- [5] Ronneberger, O., Fischer, P. and Brox, T., 2015. U-net: Convolutional networks for biomedical image segmentation. In *Medical Image Computing and Computer-Assisted Intervention—MICCAI 2015: 18th International Conference, Munich, Germany, October 5-9, 2015, Proceedings, Part III* 18 (pp. 234-241). Springer International Publishing.
- [6] K. He, X. Zhang, S. Ren, and J. Sun, Deep residual learning for image recognition, in *CVPR*, 2016, pp. 770-778 (2016)
- [7] Sundaresan, V., Zamboni, G., Rothwell, P.M., Jenkinson, M. and Griffanti, L., 2021. Triplanar ensemble U-Net model for white matter hyperintensities segmentation on MR images. *Medical image analysis*, 73, p.102184.
- [8] Sanghyun Woo, Jongchan Park, Joon-Young Lee, and In So Kweon. Cbam: Convolutional block attention module. In *The European Conference on Computer Vision (ECCV)* (2018)
- [9] Guo, C., Szemenyei, M., Yi, Y., Wang, W., Chen, B. and Fan, C., 2021, January. Sa-unet: Spatial attention u-net for retinal vessel segmentation. In *2020 25th international conference on pattern recognition (ICPR)* (pp. 1236-1242). IEEE.
- [10] Chen, L.C., Papandreou, G., Kokkinos, I., Murphy, K. and Yuille, A.L., 2017. Deeplab: Semantic image segmentation with deep convolutional nets, atrous convolution, and fully connected crfs. *IEEE transactions on pattern analysis and machine intelligence*, 40(4), pp.834-848.
- [11] Wu, Y. and He, K., 2018. Group normalization. In *Proceedings of the European conference on computer vision (ECCV)* (pp. 3-19).
- [12] Çiçek, Ö., Abdulkadir, A., Lienkamp, S.S., Brox, T. and Ronneberger, O., 2016. 3D U-Net: learning dense volumetric segmentation from sparse annotation. In *Medical Image Computing and Computer-Assisted Intervention—MICCAI 2016: 19th International Conference, Athens, Greece, October 17-21, 2016, Proceedings, Part II* 19 (pp. 424-432). Springer International Publishing.
- [13] Oktay, O., Schlemper, J., Folgoc, L.L., Lee, M., Heinrich, M., Misawa, K., Mori, K., McDonagh, S., Hammerla, N.Y., Kainz, B. and Glocker, B., 2018. Attention u-net: Learning where to look for the pancreas. *arXiv preprint arXiv:1804.03999*.